ISSN 0031-918X, Physics of Metals and Metallography, 2024, Vol. 125, No. 2, pp. 118–123. © Pleiades Publishing, Ltd., 2024.

ELECTRICAL AND MAGNETIC PROPERTIES

Transverse Magneto-Optical Kerr Effect Enhancement in Si–Ni Nanogratings by Mie and Surface Lattice Resonances

K. A. Mamian[a, *], A. Yu. Frolov[a], V. V. Popov[a], and A. A. Fedyanin[a]

[a] *Lomonosov Moscow State University, Faculty of Physics, Moscow, 119991 Russia*

**e-mail: mamyan@nanolab.phys.msu.ru*

Received September 7, 2023; revised November 9, 2023; accepted November 14, 2023

Abstract—We demonstrate experimentally that a one-dimensional array of silicon nanowires periodically placed on a nickel substrate enhances the transverse magneto-optical Kerr effect (TMOKE) compared to a nickel film. The enhancement mechanism is associated with the excitation of two types of resonances: multipole Mie resonances in each nanowire and surface lattice resonances (SLRs) emerging from the periodic arrangement of the nanowires. The maximal TMOKE values reached up to 1.9 and 2.6% due to the excitation of SLR and a magnetic dipole resonance, respectively. When the SLR is excited, the spectral width of the TMOKE enhancement is narrower compared to the case of the magnetic dipole resonance.

Keywords: magnetooptics, nanophotonics, Mie resonances, transverse magneto-optical Kerr effect, surface lattice resonance

DOI: 10.1134/S0031918X23603074

INTRODUCTION

The magneto-optical Kerr effects represent the phenomena occurring when light changes its properties after interaction with magnetized media [1]. In the case of transverse magneto-optical Kerr effect (TMOKE) the magnetization vector of the medium is perpendicular to the plane of light incidence and reflected light intensity and phase are modulated. In this case, when an external magnetic field is applied to the material, its dielectric permittivity tensor becomes non-diagonal due to spin-orbit interaction:

$$\hat{\varepsilon} = \begin{pmatrix} \varepsilon_1 & ig & 0 \\ -ig & \varepsilon_1 & 0 \\ 0 & 0 & \varepsilon_1 \end{pmatrix}, \quad (1)$$

where $\varepsilon_1 = \varepsilon_1' + i\varepsilon_1''$ is the diagonal component of the tensor, $g = g' + ig''$ is the gyration constant of the material. The value of the effect is calculated using the following equation:

$$\delta = 2 \times \frac{R(H) - R(-H)}{R(H) + R(-H)}, \quad (2)$$

where $R(H)$ and $R(-H)$ are the reflectances at opposite magnetization directions, respectively.

The TMOKE values in the most common magneto-optically active metals (Fe, Co, Ni) are too small for practical applications. The TMOKE in the optical and near-infrared spectral ranges is smaller than 0.5% for nickel films [2]. One of the ways to enhance the magneto-optical response of the material is to excite optical resonances which localize the electromagnetic fields in the magnetic materials. Such enhancement can be caused, for instance, by the excitation of localized surface plasmons (LSPs), which are resonant oscillations of free electrons of a metal particle excited by an external electromagnetic field [3–5].

Besides LSPs, surface plasmon-polaritons (SPPs), which are electromagnetic waves propagating along the metal-dielectric boundary [6], can also be used for enhancement. SPP-caused enhancement is possible, for example, in multilayered films [7, 8] and magnetoplasmonic crystals [9–16]. The enhancement mechanism in this case is the spectral shift of the resonant feature in the spectrum (maximum or minimum) corresponding to the surface plasmon resonance when the magnetic field is applied in opposite directions. However, surface plasmon resonances have disadvantages including high optical absorption in the metal, that limit their Q-factor. The use of noble metals reduces the absorption losses but weakens the interaction of light with the magnetized medium [17–21]. The enhancement of magneto-optical response in other magneto-optical materials such as magnetic dielectrics has also been demonstrated [22–24].

An alternative approach to magneto-optical effects enhancement is to use optical resonances in dielectric nanostructures. Particularly, Mie resonances—multipole scattering resonances—have gained wide attention in recent years [25, 26]. Their nature is determined by the geometrical parameters and material of

the nanostructures, and the properties of the medium. These resonances efficiently localize the electromagnetic field in subwavelength spatial volumes [27, 28].

By combining a magneto-optically active material with a resonant dielectric nanostructure, magneto-optical effects can be significantly enhanced. This has been demonstrated in the case of an array of silicon nanodiscs covered by a nickel film and deposited on a glass substrate [29–31].

The periodical arrangement of Mie resonant particles enables the excitation of collective modes that have a significantly higher Q-factor compared to individual resonances [32, 33]. The coupling of the resonances in the collective mode can be implemented by the Rayleigh anomaly (RA), which occurs when one of the diffraction orders propagates along the surface of the periodic array. The RA can spectrally overlap with the nanoparticle optical modes forming a surface lattice resonance (SLR) [34]. By means of SLR, it is possible to enhance the magneto-optical effects in two-dimensional arrays of nickel nanodiscs [35], as well as gold nanodiscs embedded in a magnetic dielectric matrix [36, 37].

In this paper, the efficiencies of Mie and SLR resonances in terms of TMOKE enhancement in a hybrid nanostructure consisting of a periodic array of rectangular amorphous silicon nanowires placed on a nickel substrate are compared.

SAMPLES

A scheme of the Si–Ni nanograting cross-section is presented in Fig. 1a. Preliminary simulations were carried out in the Ansys Lumerical FDTD software package [38] using the finite-difference time-domain method before the fabrication of the samples. The geometrical parameters of the structure were optimized to ensure that the Mie resonances are excited in the visible and near-infrared spectral ranges. The choice of silicon is motivated by its high refractive index ($n \approx 3.5$) [39] in the optical and near-infrared spectral ranges, while nickel has a large gyration constant [40].

The samples were fabricated by lift-off and electron-beam lithography techniques. They were characterized by atomic force microscopy (AFM, the image and the one-dimensional cross-section of the image along the dashed line are shown in Fig. 1b) and scanning electron microscopy (SEM, Fig. 1c). The substrate is a 200 nm thick nickel film deposited on glass. Nickel was deposited by the electrotyping technique. The design parameters of the samples are the following: width 215 nm, height 180 nm, period 700 nm. The period of the nanograting is large enough to exclude the near-field interaction between the nanowires and to ensure the presence of the RA spectrally overlapping with the Mie resonances of the individual nanowires. These parameters are averaged since they vary slightly along the axis of the nanowires due to the specifics of fabrication process.

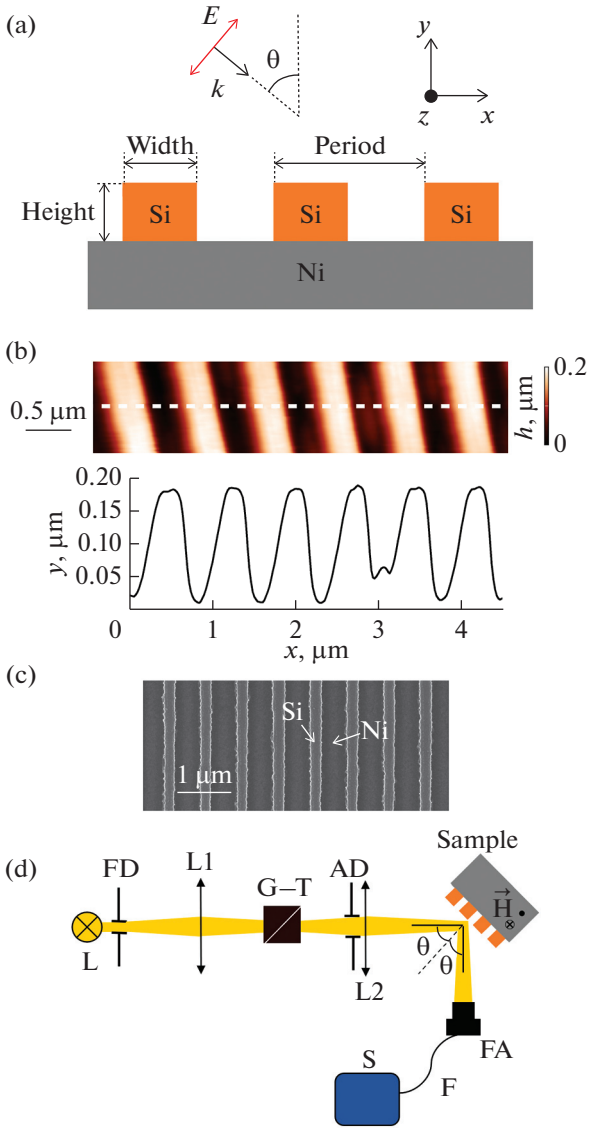

Fig. 1. (a) Scheme of the sample cross-section. (b) AFM image of the sample (top) and its cross-section along the dashed line (bottom). (c) SEM image of the sample. (d) Experimental setup scheme: L, lamp; FD, field diaphragm; L1, lens 1; G–T, Glan–Taylor prism; AD, aperture diaphragm; L2, lens 2; FA, optical fiber adapter; F, optical fiber; S, spectrometer.

EXPERIMENTAL SETUP AND NUMERICAL METHODS

The experimental setup scheme for measuring reflectance spectra and TMOKE is shown in Fig. 1d. A spectrally broadband halogen lamp is used as a light source. The beam from the lamp passes through a system of diaphragms and lenses, as well as a Glan–Taylor prism. The polarization of light is perpendicular to

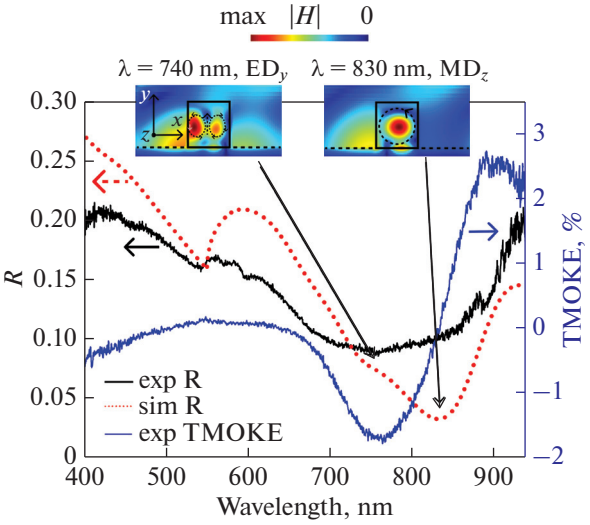

Fig. 2. Reflectance spectra (black continuous curve—experiment, red dashed curve—simulation), experimental TMOKE spectrum (blue curve) at an angle of incidence of θ = 35°, |*H*| distributions at the wavelengths of 740 and 830 nm. Dashed curves with arrows on the magnetic field distributions indicate the directions of the electric field.

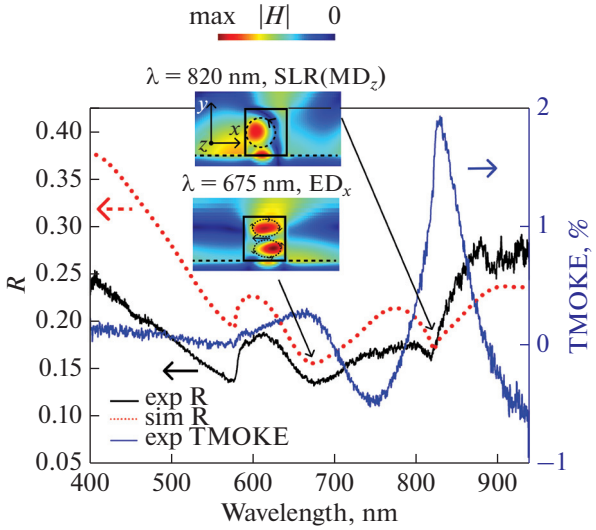

Fig. 3. Reflectance spectra (black continuous curve—experiment, red dashed curve—simulation, experimental TMOKE spectrum (blue curve) at an angle of incidence of θ = 10°, |*H*| distributions at the wavelengths of 675 and 820 nm. Dashed curves with arrows on the magnetic field distributions indicate the directions of the electric field.

the axis of the nanowires (*p*-polarization). The sample is fixed on a goniometer, which controls the angle of light incidence θ. The spectrum of the reflected light is registered by the spectrometer. To magnetize the sample, we use a static external magnetic field created by two magnets (made of an alloy of neodymium, iron, and boron) of opposite polarities. The magnetic field strength is 650 gauss at the point of beam incidence. The diameter of the beam on the sample is about 1–2 mm. The magnets are disc-shaped with a diameter of 20 mm, and the gradient of their magnetic field in the area of the beam is negligible. The external magnetic field is parallel to the axis of the nanowires and perpendicular to the plane of light incidence, which corresponds to the geometry of TMOKE.

All simulations of reflectance spectra and the magnetic near-field distributions presented below were also carried out in the Ansys Lumerical FDTD software package. Bloch periodic boundary conditions were used in the simulation to model the periodicity, and a model of electromagnetic plane wave was used as the source of radiation. The dielectric permittivity for amorphous silicon was taken from Ref. [39] and for nickel from Ref. [40].

RESULTS

To observe both individual Mie resonances and collective SLRs the reflectance and TMOKE spectra were measured at two angles of incidence: θ = 35° and θ = 10° in the spectral range of 400–940 nm (Figs. 2 and 3). Simulated reflectance spectra were also obtained. The RA associated with the –1st diffraction order occurs at θ = 10° within the considered spectral range and can excite the SLR, in contrast to the case of θ = 35° when the RA of the 1st order is observed at the wavelength of 1100 nm, which is beyond the spectral range under consideration.

Figure 2 shows the simulated and experimental reflectance spectra, as well as the experimental TMOKE spectrum at θ = 35°. Two minima are observed at the wavelengths of 740 and 830 nm in the simulated reflectance spectrum.

To understand the origin of these minima, the simulated near-field distributions of the magnetic field absolute value strength were obtained. The field distribution for the minimum at the wavelength of 740 nm shows the excitation of an electric dipole mode the moment of which is directed along the *y*-axis (ED$_y$). Hereinafter the direction of the electric field vector in the near-field distributions is schematically shown by dashed curves with arrows. This minimum corresponds to the TMOKE value of δ = –1.6%. Similarly, the minimum at the wavelength of 830 nm is explained by the magnetic dipole mode excitation MD$_z$ with a dipole moment directed along the *z*-axis. The excitation of this optical mode yields the largest TMOKE value of 2.6%. The enhancement at this angle of incidence is caused by the excitation of individual Mie resonances (ED$_y$ and MD$_z$) in silicon nanowires. These resonances localize the electromagnetic field near nickel more efficiently compared to unstructured nickel surface, resulting in TMOKE enhancement.

The reflectance and TMOKE spectra at θ = 10° are shown in Fig. 3. A minimum at the wavelength of

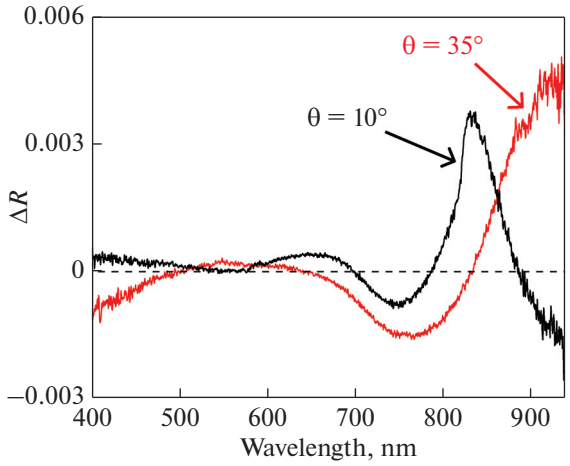

Fig. 4. Experimental FOM (ΔR) spectra at $\theta = 10°$ (black curve) and $\theta = 35°$ (red curve).

675 nm is observed in the reflectance spectra. It was established that the electric dipole mode ED_x is excited, the dipole moment of which is directed along the x-axis, see the distribution of $|H|$ in Fig. 3. This resonance corresponds to a maximal value of 0.3% in the TMOKE spectrum.

At an angle of incidence $\theta = 10°$ the RA is formed by the 1st diffraction order propagating along the surface of the nanograting at the wavelength of 820 nm. This RA spectrally overlaps with the magnetic dipole mode MD_z with a dipole moment directed along the z-axis (as shown by the corresponding distribution of $|\bar{H}|$), exciting the SLR (MD_z). The SLR excitation results in a dip in the reflectance spectrum. The greater Q-factor of this resonance compared to the rest individual optical modes is due to the overlap of a wideband resonance (namely, magnetic dipole MD_z) and a narrowband one (RA related to -1 order of diffraction). We observe a peak in the TMOKE spectrum, reaching up to 1.9% in this spectral region.

Thus, an individual magnetic dipole mode MD_z leads to a larger TMOKE value compared to SLR, which shows its potential in light intensity modulation. At the same time, the TMOKE peak is much narrower in the case of an SLR-induced enhancement, which is important for magneto-optical sensing [41–46].

An important feature of TMOKE above and beyond δ is the figure of merit value (FOM), defined as follows:

$$\Delta R = \delta R. \quad (3)$$

The comparison of experimental ΔR spectra at the angles of incidence $\theta = 10°$ and $\theta = 35°$ is presented in Fig. 4.

One can see that the greater value of ΔR is achieved at a larger angle of incidence in the spectral vicinity of both the ED resonance (from 700 to 800 nm) and the MD resonance (from 800 to 940 nm). Thus, the excitation of an individual Mie resonance without SLRs is optimal from the point of view of both the magnitudes of δ and ΔR.

CONCLUSIONS

It has been experimentally shown that the transverse magneto-optical Kerr effect values in Si–Ni nanogratings made of rectangular nanowires are larger in the case of an individual Mie resonance excitation compared to the case of the surface lattice resonances (SLRs). The maximal value of TMOKE in the case of SLR is 1.9%, while it reaches up to 2.6% if an individual magnetic dipole Mie resonance is excited.

The obtained TMOKE values are almost an order of magnitude larger than the typical ones for the unstructured nickel film, which do not exceed 0.5% in the considered spectral range [2]. However, the spectral width of the TMOKE resonance at the SLR is narrower compared to the case of the individual Mie resonance excitation. Thus, the same nanograting can be used both as a light modulator and as a magneto-optical sensor if the angle of light incidence is changed.

ACKNOWLEDGEMENTS

The authors are grateful to O.V. Snigirev and I.V. Bozhev for their assistance in sample fabrication.

FUNDING

The work was supported by the BASIS Foundation through Grant no. 23-2-9-11-1 (simulations of the reflectance spectra and distributions of the electromagnetic fields of optical modes), grant of the Russian Science Foundation no. 20-12-00389 (experimental measurements), and the MSU Interdisciplinary Scientific and Educational School "Photonic and Quantum technologies. Digital medicine" (sample fabrication).

CONFLICT OF INTEREST

The authors of this work declare that they have no conflicts of interest.

REFERENCES

1. A. K. Zvezdin and V. A. Kotov, *Modern Magnetooptics and Magnetooptical Materials* (CRC Press, 1997). https://doi.org/10.1201/9780367802608
2. G. S. Krinchik and V. A. Artem'ev, "Magneto-optical properties of Ni, Co, and Fe in the ultraviolet visible and infrared parts of the spectrum," Sov. Phys. JETP, 1080–1085 (1968).
3. S. A. Maier, *Plasmonics: Fundamentals and Applications* (Springer, New York, 2007). https://doi.org/10.1007/0-387-37825-1
4. G. Armelles, J. B. González-Díaz, A. García-Martín, J. M. García-Martín, A. Cebollada, M. U. González,

S. Acimovic, J. Cesario, R. Quidant, and G. Badenes, "Localized surface plasmon resonance effects on the magneto-optical activity of continuous Au/Co/Au trilayers," Opt. Express **16**, 16104–16112 (2008). https://doi.org/10.1364/oe.16.016104

5. L. Wang, K. Yang, C. Clavero, A. J. Nelson, K. J. Carroll, E. E. Carpenter, and R. A. Lukaszew, "Localized surface plasmon resonance enhanced magneto-optical activity in core-shell Fe–Ag nanoparticles," J. Appl. Phys. **107**, 09B303 (2010). https://doi.org/10.1063/1.3355905
6. W. L. Barnes, A. Dereux, and T. W. Ebbesen, "Surface plasmon subwavelength optics," Nature **424**, 824–830 (2003). https://doi.org/10.1038/nature01937
7. V. I. Safarov, V. A. Kosobukin, C. Hermann, G. Lampel, J. Peretti, and C. Marlière, "Magneto-optical effects enhanced by surface plasmons in metallic multilayer films," Phys. Rev. Lett. **73**, 3584–3587 (1994). https://doi.org/10.1103/physrevlett.73.3584
8. C. Clavero, K. Yang, J. R. Skuza, and R. A. Lukaszew, "Magnetic field modulation of intense surface plasmon polaritons," Opt. Express **18**, 7743–7752 (2010). https://doi.org/10.1364/OE.18.007743
9. Yu. Takashima, M. Haraguchi, and Yo. Naoi, "Numerical finite-difference time-domain calculation for extreme enhancement of magneto-optical effect at ultraviolet wavelength using Ni-subwavelength grating on SiO\2/Ni structure," Opt. Rev. **29**, 62–67 (2022). https://doi.org/10.1007/s10043-021-00711-2
10. M. A. Kiryanov, G. S. Ostanin, T. V. Dolgova, M. Inoue, and A. A. Fedyanin, "Anomalous picosecond optical transmittance dynamics in Au–Bi:YIG hybrid metasurface," JETP Lett. **117**, 196–201 (2023). https://doi.org/10.1134/s0021364022603220
11. V. B. Novikov, A. M. Romashkina, D. A. Ezenkova, I. A. Rodionov, K. N. Afanasyev, A. V. Baryshev, and T. V. Murzina, "Surface plasmon driven enhancement of linear and nonlinear magneto-optical Kerr effects in bimetallic magnetoplasmonic crystals in conical diffraction," Phys. Rev. B **105**, 155408 (2022). https://doi.org/10.1103/physrevb.105.155408
12. A. R. Pomozov, A. L. Chekhov, I. A. Rodionov, A. S. Baburin, E. S. Lotkov, M. P. Temiryazeva, K. N. Afanasyev, A. V. Baryshev, and T. V. Murzina, "Two-dimensional high-quality Ag/Py magnetoplasmonic crystals," Appl. Phys. Lett. **116**, 013106 (2020). https://doi.org/10.1063/1.5135711
13. I. A. Novikov, M. A. Kiryanov, P. K. Nurgalieva, A. Yu. Frolov, V. V. Popov, T. V. Dolgova, and A. A. Fedyanin, "Ultrafast magneto-optics in nickel magnetoplasmonic crystals," Nano Lett. **20**, 8615–8619 (2020). https://doi.org/10.1021/acs.nanolett.0c03305
14. M. A. Kiryanov, A. Yu. Frolov, I. A. Novikov, P. A. Kipp, P. K. Nurgalieva, V. V. Popov, A. A. Ezhov, T. V. Dolgova, and A. A. Fedyanin, "Surface profile-tailored magneto-optics in magnetoplasmonic crystals," APL Photonics **7**, 26104 (2022). https://doi.org/10.1063/5.0072698
15. A. Yu. Frolov, M. R. Shcherbakov, and A. A. Fedyanin, "Dark mode enhancing magneto-optical Kerr effect in multilayer magnetoplasmonic crystals," Phys. Rev. B **101**, 045409 (2020). https://doi.org/10.1103/physrevb.101.045409
16. S. A. Dyakov, I. M. Fradkin, N. A. Gippius, L. Klompmaker, F. Spitzer, E. Yalcin, I. A. Akimov, M. Bayer, D. A. Yavsin, S. I. Pavlov, A. B. Pevtsov, S. Y. Verbin, and S. G. Tikhodeev, "Wide-band enhancement of the transverse magneto-optical Kerr effect in magnetite-based plasmonic crystals," Phys. Rev. B **100**, 214411 (2019). https://doi.org/10.1103/physrevb.100.214411
17. Q. Wang, H. Yao, Ye. Feng, X. Deng, B. Yang, D. Xiong, M. He, and W. Zhang, "Surface plasmon resonances boost the transverse magneto-optical Kerr effect in a CoFeB slab covered by a subwavelength gold grating for highly sensitive detectors," Opt. Express **29**, 10546–10555 (2021). https://doi.org/10.1364/oe.414749
18. T. Cheng, W. Yang, Z. Liu, H. Yu. Feng, J. Qin, Yi. Ma, S. Li, L. Bi, and F. Luo, "Enhanced Faraday rotation by a Fano resonance in substrate-free three-dimensional magnetoplasmonic structures," Nanoscale **15**, 15583–15589 (2023). https://doi.org/10.1039/d3nr02737f
19. L. V. Panina, V. K. Belyaev, A. Anikin, A. Shumskaya, A. G. Kozlov, A. V. Ognev, A. Rogachev, I. Korol'kov, M. Zdorovets, A. Kozlovskii, and V. V. Rodionova, "Nanocomposites with magnetic core–gold shell structure for photothermia," Phys. Met. Metallogr. **123**, 1185–1192 (2022). https://doi.org/10.1134/s0031918x22601597
20. S. V. Tomilin, A. B. Karavainikov, S. D. Lyashko, E. T. Milyukova, O. A. Tomilina, and V. N. Berzhanskii, "Effect of nanostructuring on excitation of different resonant modes in a magnetoplasmonic crystal," Phys. Met. Metallogr. **123**, 668–673 (2022). https://doi.org/10.1134/s0031918x22070201
21. I. A. Kolmychek, A. R. Pomozov, A. P. Leontiev, K. S. Napolskii, and T. V. Murzina, "Magneto-optical effects in Au/Ni based composite hyperbolic metamaterials," Phys. Met. Metallogr. **120**, 1266–1269 (2019). https://doi.org/10.1134/s0031918x19130131
22. A. L. Chekhov, P. N. Naydenov, M. N. Smirnova, V. A. Ketsko, A. I. Stognij, and T. V. Murzina, "Magnetoplasmonic crystal waveguide," Opt. Express **26**, 21086–21091 (2018). https://doi.org/10.1364/OE.26.021086
23. A. N. Kalish, R. S. Komarov, M. A. Kozhaev, V. G. Achanta, S. A. Dagesyan, A. N. Shaposhnikov, A. R. Prokopov, V. N. Berzhansky, A. K. Zvezdin, and V. I. Belotelov, "Magnetoplasmonic quasicrystals: An approach for multiband magneto-optical response," Optica **5**, 617–623 (2018). https://doi.org/10.1364/OPTICA.5.000617
24. L. Bsawmaii, E. Gamet, S. Neveu, D. Jamon, and F. Royer, "Magnetic nanocomposite films with photo-patterned 1D grating on top enable giant magneto-optical intensity effects," Opt. Mater. Express **12**, 513–523 (2022). https://doi.org/10.1364/ome.447030
25. C. F. Bohren and D. R. Huffman, *Absorption and Scattering of Light by Small Particles* (Wiley, 2004). https://doi.org/10.1002/9783527618156

26. A. M. Chernyak, M. G. Barsukova, A. S. Shorokhov, A. I. Musorin, and A. A. Fedyanin, "Bound states in the continuum in magnetophotonic metasurfaces," JETP Lett. **111**, 46–49 (2020). https://doi.org/10.1134/s0021364020010105

27. A. I. Kuznetsov, A. E. Miroshnichenko, M. L. Brongersma, Yu. S. Kivshar, and B. Luk'yanchuk, "Optically resonant dielectric nanostructures," Science **354**, aag2472 (2016). https://doi.org/10.1126/science.aag2472

28. L. Cao, P. Fan, E. S. Barnard, A. M. Brown, and M. L. Brongersma, "Tuning the color of silicon nanostructures," Nano Lett. **10**, 2649–2654 (2010). https://doi.org/10.1021/nl1013794

29. M. G. Barsukova, A. I. Musorin, A. S. Shorokhov, and A. A. Fedyanin, "Enhanced magneto-optical effects in hybrid Ni–Si metasurfaces," APL Photonics **4**, 16102 (2019). https://doi.org/10.1063/1.5066307

30. A. I. Musorin, M. G. Barsukova, A. S. Shorokhov, B. S. Luk'yanchuk, and A. A. Fedyanin, "Manipulating the light intensity by magnetophotonic metasurfaces," J. Magn. Magn. Mater. **459**, 165–170 (2018). https://doi.org/10.1016/j.jmmm.2017.11.049

31. M. G. Barsukova, A. S. Shorokhov, A. I. Musorin, D. N. Neshev, Yu. S. Kivshar, and A. A. Fedyanin, "Magneto-optical response enhanced by Mie resonances in nanoantennas," ACS Photonics **4**, 2390–2395 (2017). https://doi.org/10.1021/acsphotonics.7b00783

32. A. D. Utyushev, V. I. Zakomirnyi, and I. L. Rasskazov, "Collective lattice resonances: Plasmonics and beyond," Rev. Phys. **6**, 100051 (2021). https://doi.org/10.1016/j.revip.2021.100051

33. V. I. Zakomirnyi, A. E. Ershov, V. S. Gerasimov, S. V. Karpov, H. Ågren, and I. L. Rasskazov, "Collective lattice resonances in arrays of dielectric nanoparticles: A matter of size," Opt. Lett. **44**, 5743–5746 (2019). https://doi.org/10.1364/ol.44.005743

34. G. W. Castellanos, P. Bai, and J. Gómez Rivas, "Lattice resonances in dielectric metasurfaces," J. Appl. Phys. **125**, 213105 (2019). https://doi.org/10.1063/1.5094122

35. M. Kataja, T. K. Hakala, A. Julku, M. J. Huttunen, S. Van Dijken, and P. Törmä, "Surface lattice resonances and magneto-optical response in magnetic nanoparticle arrays," Nat. Commun. **6**, 7072 (2015). https://doi.org/10.1038/ncomms8072

36. I. A. Kolmychek, A. N. Shaimanov, A. V. Baryshev, and T. V. Murzina, "Magneto-optical response of two-dimensional magnetic plasmon structures based on gold nanodisks embedded in a ferrite garnet layer," JETP Lett. **102**, 46–50 (2015). https://doi.org/10.1134/s0021364015130056

37. A. V. Chetvertukhin, A. I. Musorin, T. V. Dolgova, H. Uchida, M. Inoue, and A. A. Fedyanin, "Transverse magneto-optical Kerr effect in 2D gold–garnet nanogratings," J. Magn. Magn. Mater. **383**, 110–113 (2015). https://doi.org/10.1016/j.jmmm.2014.12.062

38. Ansys Lumerical FDTD: Simulation of photonic components. https://www.ansys.com/products/photonics/fdtd.

39. D. T. Pierce and W. E. Spicer, "Electronic structure of amorphous Si from photoemission and optical studies," Phys. Rev. B **5**, 3017–3029 (1972). https://doi.org/10.1103/physrevb.5.3017

40. *Handbook of Optical Constants of Solids*, Ed. by E. D. Palik (Academic, 1985). https://doi.org/10.1016/C2009-0-20920-2

41. C. Rizal, M. G. Manera, D. O. Ignatyeva, J. R. Mejía-Salazar, R. Rella, V. I. Belotelov, F. Pineider, and N. Maccaferri, "Magnetophotonics for sensing and magnetometry toward industrial applications," J. Appl. Phys. **130**, 230901 (2021). https://doi.org/10.1063/5.0072884

42. A. A. Grunin, I. R. Mukha, A. V. Chetvertukhin, and A. A. Fedyanin, "Refractive index sensor based on magnetoplasmonic crystals," J. Magn. Magn. Mater. **415**, 72–76 (2016). https://doi.org/10.1016/j.jmmm.2016.03.069

43. V. K. Belyaev, V. V. Rodionova, A. A. Grunin, M. Inoue, and A. A. Fedyanin, "Magnetic field sensor based on magnetoplasmonic crystal," Sci. Rep. **10**, 7133 (2020). https://doi.org/10.1038/s41598-020-63535-1

44. D. Murzin, D. J. Mapps, K. Levada, V. Belyaev, A. Omelyanchik, L. Panina, and V. Rodionova, "Ultrasensitive magnetic field sensors for biomedical applications," Sensors **20**, 1569 (2020). https://doi.org/10.3390/s20061569

45. V. K. Belyaev, D. V. Murzin, N. N. Perova, A. A. Grunin, A. A. Fedyanin, and V. V. Rodionova, "Permalloy-based magnetoplasmonic crystals for sensor applications," J. Magn. Magn. Mater. **482**, 292–295 (2019). https://doi.org/10.1016/j.jmmm.2019.03.052

46. D. V. Murzin, A. Yu. Frolov, K. A. Mamian, V. K. Belyaev, A. A. Fedyanin, and V. V. Rodionova, "Low coercivity magnetoplasmonic crystal based on a thin permalloy film for magnetic field sensing applications," Opt. Mater. Express **13**, 171–178 (2023). https://doi.org/10.1364/ome.478112